Supplementary Information for "Microfluidic Magnetophoretic Separations of Immunomagnetically Labeled Rare Mammalian Cells"

Thomas P. Forbes and Samuel P. Forry

National Institute of Standards and Technology, Gaithersburg, MD, USA

Table of Contents

Nomenclature

B	Magnet field
$B*$	Characteristic magnetic field
d	Distance between the channel and magnet centerlines
D	Diffusivity
F_{mag}	Magnetic force on particle
F_{drag}	Drag force on particle
h	Magnet half height
l	characteristic length scale
m	Magnetic moment
m_b	Mass of bead
m_{cell}	Mass of cell
m_T	Mass of total complex
M_s	Saturation magnetism of the Neodymium magnet
$M_{s,b}$	Saturation magnetism of the superparamagnetic bead
M_b	Bead magnetism
N	Number of superparamagnetic beads in a cell-bead complex
N_{cell}	Number of cells in a cell-bead complex
R_p	Effective particle radius
R_{drag}	Drag radius

R_b	Bead radius
R_{cell}	Cell radius
R_T	Volumetric radius of total aggregate
t	Time
t_{res}	Residence time
U	Average free stream velocity
u	velocity
u_f	Fluid velocity
u_p	Particle velocity
u^*	Characteristic velocity
V_{mag}	Volume of the magnet
V_b	Volume of bead
w	Magnet half width
w_{ch}	Channel width
w_m	Magnet width
x	Coordinate system for magnetic field calculations
X	Coordinate system of particle trajectory
y	Coordinate system for magnetic field calculations
Z	Coordinate system of particle trajectory
z_{displ}	Lateral displacement
$\bar{Z}_{displ}$	Dimensionless lateral displacement
κ_{cell}	Non-sphericity factor of the cell
κ_b	Non-sphericity factor of the bead
κ_T	Non-sphericity factor of the total aggregate
μ_o	Permeability of free space
η	Fluid viscosity
θ	Angle of magnet relative to flow direction
χ	Magnetic susceptibility
χ_{eff}	Effective magnetic susceptibility
ρ_f	Fluid density
ρ_b	Bead density

Magnetic Force Equations

The magnetic force on a superparamagnetic bead with a uniform magnetic moment is given by:

$$\vec{F}_{mag} = (\vec{m} \cdot \vec{\nabla})\vec{B} \tag{S1}$$

Where, $\vec{B}$ is the magnetic field, and the magnetic moment is a function of the superparamagnetic bead volume and bead magnetism, $\vec{m} = \vec{M_b}V_b$. As is common in the literature, the bead magnetism, $\vec{M_b}$, is approximated as linearly increasing with the magnetic field up to the saturation magnetism.[1-7] The model accounts for the level of bead magnetism through the following factor, $f(B)$, as demonstrated in Equation S2. The bead is at its saturation magnetism in the region of high magnetic field directly over the permanent magnet.

$$\vec{M_b} = f(B)\,\vec{B}/\mu_o \tag{S2}$$

where

$$f(B) = \begin{cases} \chi_{eff} & B/\mu_o < M_{s,b}/\chi_{eff} \\ \dfrac{M_{s,b}}{B/\mu_o} & B/\mu_o \geq M_{s,b}/\chi_{eff} \end{cases} \tag{S3}$$

The magnetic force experienced by the superparamagnetic beads and labeled target cells is given by:

$$\vec{F}_{mag} = V_b f(B)(\vec{B} \cdot \vec{\nabla})\vec{B}/\mu_o \tag{S4}$$

Where V_b and χ_{eff} are the bead volume and effective magnetic susceptibility, respectively. The magnetic force on each superparamagnetic bead can be separated into components in the coordinate system defined in Figure S1.

$$F_{mag,x} = V_b f(B)/\mu_o \left[B_x(x,y)\frac{\partial B_x(x,y)}{\partial x} + B_y(x,y)\frac{\partial B_x(x,y)}{\partial y} \right] \tag{S5}$$

$$F_{mag,y} = V_b f(B)/\mu_o \left[B_x(x,y)\frac{\partial B_y(x,y)}{\partial x} + B_y(x,y)\frac{\partial B_y(x,y)}{\partial y} \right] \tag{S6}$$

The magnetic field distribution components around a rectangular magnetic element, with the origin at its center, are given by:

$$B_x(x,y) = \frac{M_s \mu_o}{4\pi}\left[\ln\left(\frac{(x+w)^2+(y-h)^2}{(x+w)^2+(y+h)^2}\right) - \ln\left(\frac{(x-w)^2+(y-h)^2}{(x-w)^2+(y+h)^2}\right)\right] \tag{S7}$$

$$B_y(x,y) = \frac{M_s \mu_o}{2\pi}\left[\tan^{-1}\left(\frac{2h(x+w)}{(x+w)^2+y^2-h^2}\right) - \tan^{-1}\left(\frac{2h(x-w)}{(x-w)^2+y^2-h^2}\right)\right] \tag{S8}$$

Here, M_s is the saturation magnetism, h and w are the magnetic element half height and half width, respectively (Figure S1). The magnet's magnetism is in the y-direction. The full set of field equations are based on, and extended from those found in Reference 1.[2-4, 8] A representative magnetic field distribution is shown in Figure S1(b), as calculated for a single permanent magnetic element from Equations S7-S8.
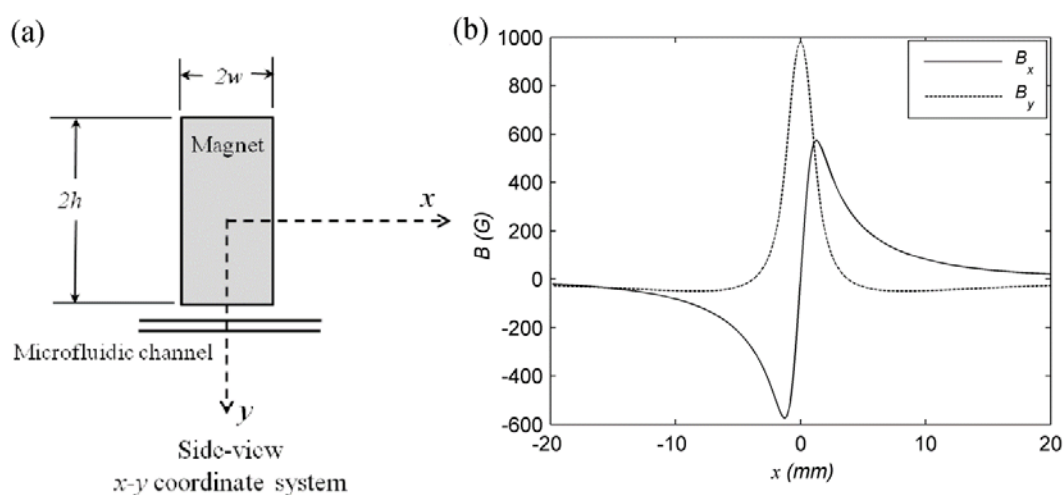

FIG. S1. (a) Schematic representation the magnet above a microfluidic channel, showing coordinate system for magnetic field calculations. (b) Representative magnetic field distribution within a microfluidic channel adjacent to a NdFeB magnet centered at the origin.

Numerical Magnetophoresis Simulation Results

The numerical model is used to demonstrate superparamagnetic bead displacement for a number of system variables. Particle trajectories are solved in a transformed coordinate axis as displayed in Figure S2. As described in the article text, the model incorporates lateral displacement for solo magnetic beads and cell-bead complexes, modeled as spheres with an effective drag radius and magnetic susceptibility.
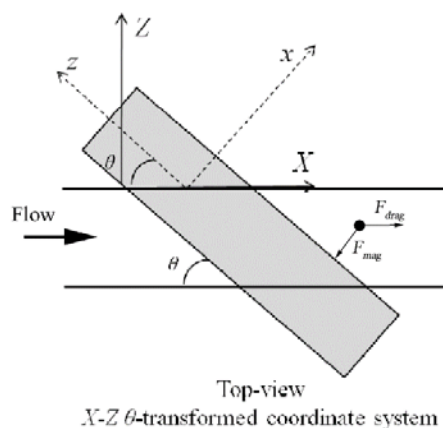
FIG. S2. Coordinate transformation for particle trajectory modeling.

Solo Bead Results

Figure S3 demonstrates the magnetophoretic displacement across the microfluidic channel as a function of (a) distance between magnet and channel, (b) magnet angle relative to the flow direction for solo superparamagnetic beads.
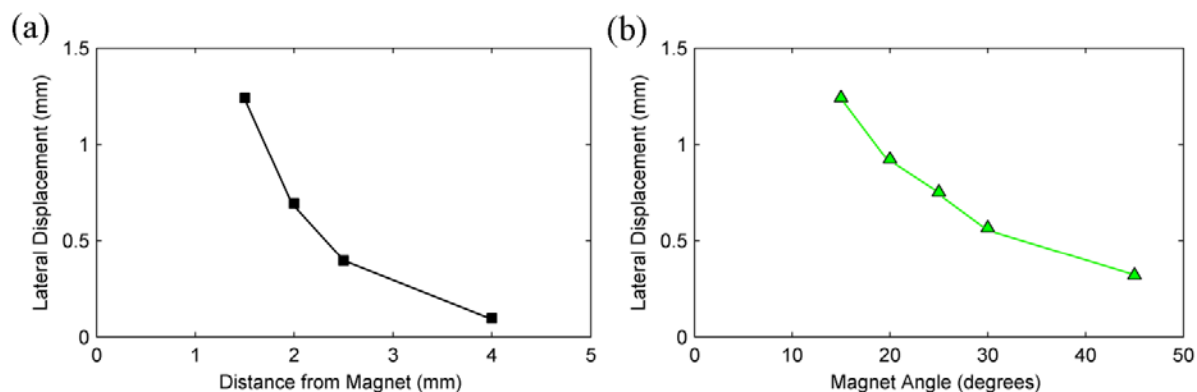

FIG. S3. (Color online) Simulated lateral deflection as a function of (a) distance from the magnet surface and (b) magnet angle relative to the flow direction, for 3.5 μm (radius) solo beads. All other system parameters are the baseline values provided in the article text.

Bead-Cell Complex Results

Corrections for total complex mass and effective Stokes drag radius are incorporated for cell-bead complexes. The total complex mass, given below, replaces the particle mass, m_p, in Equations (4a) and (4b) in the text.

$$m_T = N_{cell} m_{cell} + N m_b \tag{S9}$$

R_{drag} is based on an "effective" Stokes radius for an aggregate of spherical particles of different diameter as developed by Stober *et al.* and Okuyama *et al.*[9, 10]

$$R_{drag} = \frac{\left\{ \left[R_{cell}\kappa_{cell}^{1/2} \right]^3 + \left[R_p\kappa_b^{1/2} \right]^3 \right\}^{1/3}}{\kappa_T^{1/2}}$$ (S10)

As defined by Stober *et al.*, κ is a measure of the "non-sphericity" of the aggregate. Here, $\kappa_i = R_T^2/R_i^2$, for the bead, cell, and total complex; and R_T is the volumetric radius of the total aggregate, $\left(R_T = \left(N_{cell}R_{cell}^3 + NR_b^3 \right)^{1/3} \right)$. Figure S4 displays the simulated cell-bead complex trajectory and lateral deflection across the channel for a 10 μm (radius) cell bound by 'N' superparamagnetic beads. In addition, Figure S5 demonstrates the magnetophoretic displacement across the microfluidic channel as a function of (c) cell size, and (d) number of cells bound to a solo bead for complexes.
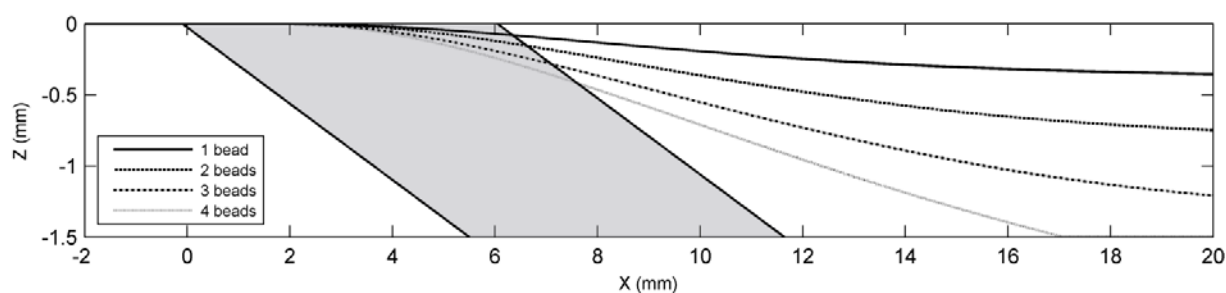

FIG. S4. Numerical simulations of trajectories for cell-bead complexes with 3.5 μm superparamagnetic beads bound to a 10 μm (radius) cell at a buffer flow rate of 13 ml/hr.
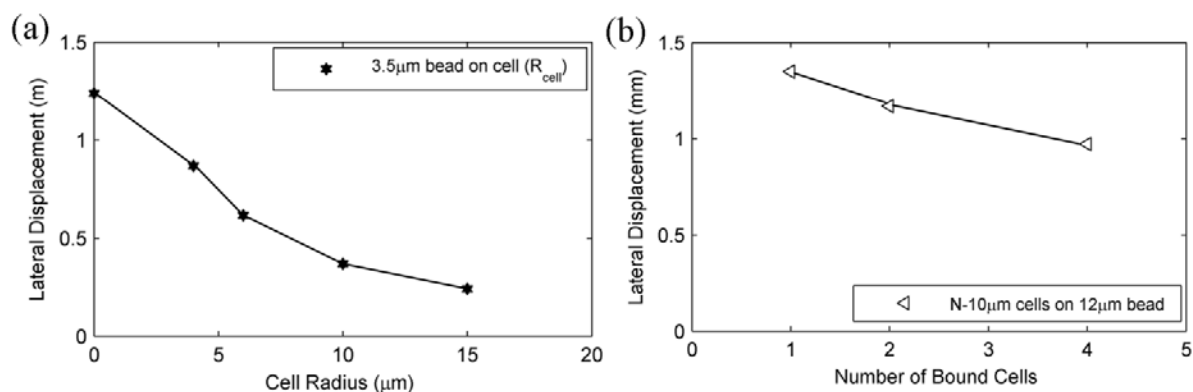

FIG. S5. Simulated lateral deflection for cell- bead complexes (a) as a function of cell size and (b) for a single 12 μm superparamagnetic bead bound by 10 μm cells, for cell-bead complexes. All other system parameters are the baseline values provided in the article text.

Scaling Analysis

As introduced in the article text, non-dimensionalizing the governing equation for particle motion (Equation (1)) with the appropriate characteristic scales for the magnetic and drag forces allows us to derive the dimensionless magnetophoresis parameter, Π_{mag}. Neglecting the transient term, the dimensionless magnetophoresis parameter is defined by a balance of the magnetic and drag forces in the direction perpendicular to the magnet (*x*-coordinate, Figure S2),

$$m_p \frac{d\vec{u}_p}{dt} = \vec{F}_{mag} + \vec{F}_{drag}$$

$$0 = \frac{NV_b \chi_{eff}}{\mu_o}(\vec{B} \cdot \vec{\nabla})\vec{B} + 6\pi \eta R_{drag} \sin \theta (\vec{u}_p - \vec{u}_f) \tag{S11}$$

The velocity and magnetic field are normalized by the average linear velocity, $u^* \sim U$, and characteristic magnetic field, $B^* \sim \mu_o M_s V_{mag}/4\pi d^3$, as shown here. The characteristic magnetic field is spatially only a function of the distance from channel centerline to magnet center, *d*. Therefore, the gradient of the characteristic magnetic field is approximated as, $\vec{\nabla} B^* \sim \partial B^*/\partial d$. Now, the magnetic field and its gradient can be approximated as a function of the permeability of free space, the NdFeB magnet's volume and saturation magnetism, and the distance from the magnet. This eliminates the need to have an exact measurement of $(\vec{B} \cdot \vec{\nabla})\vec{B}$ to estimate the regime of operation. $(\ )'$ denotes a dimensionless variable.

$$\vec{B}' = \frac{\vec{B}}{B^*} = \frac{\vec{B}}{\mu_o M_s V_{mag}/4\pi d^3} \tag{S12a}$$

$$\vec{\nabla}\vec{B}' = \frac{\vec{\nabla}\vec{B}}{\vec{\nabla}B^*} = \frac{\vec{\nabla}\vec{B}}{-3\mu_o M_s V_{mag}/4\pi d^4} \tag{S12b}$$

$$\vec{u}_p' = \frac{\vec{u}_p}{U} \tag{S12c}$$

$$\vec{u}_f' = \frac{\vec{u}_f}{U} \tag{S12d}$$

Inserting into Equation (S11),

$$0 = \left[\frac{-3N\left(\frac{4}{3}\pi R_p^3\right)\chi_{eff}\mu_o M_s^2 V_{mag}^2}{16\pi^2 d^7} \right](\vec{B}' \cdot \vec{\nabla})\vec{B}' + \left[6\pi \eta R_{drag} \sin \theta \, U \right](\vec{u}_p' - \vec{u}_f') \tag{S13}$$

Dividing through by $6\pi \eta R_{drag} \sin \theta \, U$,

$$0 = \underbrace{\left(\frac{-3 \cdot \frac{4}{3}\pi}{16\pi^2 \cdot 6\pi}\right)}_{\substack{Dimensionless \\ constants}} \underbrace{\left[\frac{NR_p^3 \chi_{eff} \mu_o M_s^2 V_{mag}^2}{\eta R_{drag} \sin\theta U d^7}\right]}_{\substack{Magnetophoresis \\ Parameter \\ "\Pi_{mag}"}} \underbrace{(\vec{B}' \cdot \vec{\nabla})\vec{B}'}_{\substack{Dimensionless \\ O(1)}} + \underbrace{(\vec{u}_p' - \vec{u}_f')}_{\substack{Dimensionless \\ O(1)}} \tag{S14}$$

$$\Pi_{mag} = \frac{N\chi_{eff} R_p^3 \mu_o M_s^2 V_{mag}^2}{\eta R_{drag} \sin\theta U d^7} \tag{S15}$$

This term clearly demonstrates that increases in the number of beads, bead size, effective magnetic susceptibility, magnet strength, and magnet volume will increase the relative magnetic-to-hydrodynamic effects. While, increases in the fluid viscosity, effective drag radius, flow velocity, magnet angle, or magnet-channel separation will decrease the relative magnetic-to-hydrodynamic effects.

Experimental Results

Methods and Materials

The microfluidic device consists of two inlets (sample and buffer) to provide a confining flow, a single flow channel, and three outlets for collection corresponding to increasing levels of magnetic deflection. The device is fabricated by polydimethylsiloxane (PDMS, Sylgard 184 silicone elastomer kit, Dow Corning, Midland, MI, USA) (certain commercial products are identified in order to adequately specify the experimental procedure; this does not imply endorsement or recommendation by NIST, nor does it imply that such products are necessarily the best available for the purpose) molding and plasma bonded to a glass slide. The master is fabricated from double sided tape using a razor cutter (FC8000, Graphtec America, Inc., Irvine, CA, USA). Alignment marks for the permanent magnet placement are incorporated into the master ($\pm$ 2°). The resulting PDMS layer is 3.0 ± 0.2 mm thick and the microfluidic channel is 1.50 ± 0.05 mm wide and 120 ± 20 µm high.

The sample and buffer are pumped through the two inlets at constant flow rates by separate syringe pumps (Dual-syringe infusion/withdrawal pump, Cole-Parmer, Vernon Hills, IL, USA). The relative widths of sample and buffer flows within the channel are determined by the relative flow rates of each. Initial experiments are completed with 3.56 ± 0.42 µm radius superparamagnetic beads

(Streptavidin coated magnetic polystyrene microspheres, C-MAGPS-6.0Av, Corpuscular Inc., Cold Spring, NY, USA), 2.07 ± 0.32 μm radius superparamagnetic beads (Coated polystyrene magnetic particles, streptavidin, PMSt-4, Discovery Scientific, Inc., Vancouver, BC, Canada), and a 25.4 mm × 6.35 mm × 1.59 mm Neodymium (NdFeB) magnet (K&J Magnetics Inc., Jamison, PA, USA).

Cell binding experiments are completed with the same 3.5 μm radius superparamagnetic beads, which have a binding capacity of 0.12 nmole biotin-FITC to 1 mg of beads. The streptavidin coated superparamagnetic beads are functionalized by incubation with biotinylated anti-EpCAM antibody (EpCAM antibody [VU-1D9] (biotin), ab79079, Abcam, Cambridge, MA, USA). EpCAM (epithelial cell adhesion molecule) is a surface antigen expressed in epithelial cells and most circulating tumor cells, which includes MCF-7. The breast adenocarcinoma MCF-7 cells (American type Culture Collection (ATCC), Manassas, VA) are grown in Dulbecco's modified Eagle's Minimum Essential Medium (ATCC), supplemented with 0.01 mg/ml bovine insulin and a volume fraction of 10% fetal bovine serum. The MCF-7 cell line is cultured to ≈80% confluence and harvested using a mass concentration of 0.25% trypsin solution. The anti-EpCAM antibody coated superparamagnetic beads (1×10^6 beads/ml) are mixed with harvested MCF-7 cells (5×10^4 cells/ml to 1×10^5 cells/ml) in suspension on a rotating mixer for 60 minutes prior to experiments.

Magnetophoresis Results

The PDMS device used for experimental validation of the numerical model is shown in Figure S4(a). Specifics of the device fabrication and materials are given in the article. Also as discussed in the article text, displacement measurements are taken from bright field images of the microfluidic channel using the NIH *ImageJ* software (http://rsbweb.nih.gov/ij/). For the small solo beads, images are taken with long exposure times, i.e., 10 ms to 50 ms, so that beads flowing with the fluid are easily identifiable streaks in the image. Figure S6 displays the magnetophoretic deflection measurements for two magnet angles and two bead sizes as a function of the average flow rate. Alternatively, for MCF-7 cell-bead

complex displacement measurements, a higher magnification is used and images are taken with very short
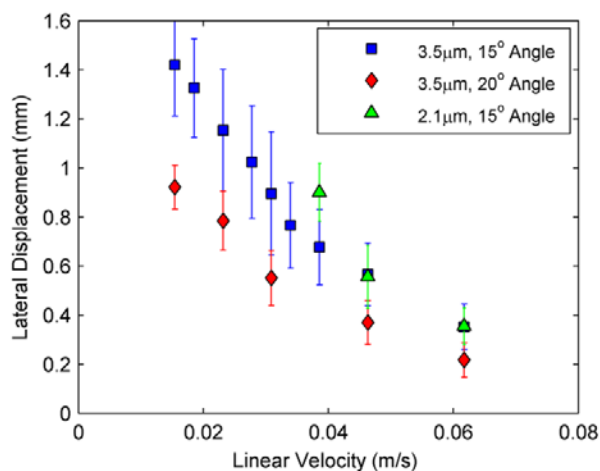
exposure times.

FIG. S6. (Color online) Experimental measurements of lateral deflection as a function of linear velocity of the buffer. Data are for magnet angles of 15° and 20° relative to the flow direction and 3.5 μm and 2.0 μm beads. All other system parameters are the baseline values provided in the text. Data points and error bars represent the average values and standard deviations, respectively, of the results obtained from 20 to 100 experimental measurements from 5 images of bead deflection at each set of conditions.

FIG. S7. PDMS microfluidic device for magnetophoretic displacement measurements.

References

1. Z. Fan and R. Kumar, *Biochip Technology*, Hardwood Academic Publishers, Philadelphia, PA, 2001.
2. E. Furlani, Y. Sahoo, K. Ng, J. Wortman and T. Monk, *Biomedical Microdevices*, 2007, **9**, 451-463.
3. E. P. Furlani, *Permanent Magnet and Electromechanical Devices; Materials, Analysis and Applications*, Academic, New York, 2001.
4. E. P. Furlani, *Journal of Applied Physics*, 2006, **99**, 024912-024911.
5. E. E. Keaveny and M. R. Maxey, *Journal of Computational Physics*, 2008, **227**, 9554-9571.
6. S. S. Shevkoplyas, A. C. Siegel, R. M. Westervelt, M. G. Prentiss and G. M. Whitesides, *Lab on a Chip*, 2007, **7**, 1294-1302.
7. B. B. Yellen and G. Friedman, *Journal of Applied Physics*, 2003, **93**, 8447-8449.
8. E. P. Furlani and K. C. Ng, *Physical Review E*, 2006, **73**, 061919.
9. K. Okuyama, Y. Kousaka and A. C. Payatakes, *Journal of Colloid and Interface Science*, 1981, **81**, 21-31.
10. W. Stober, A. Berner and R. Blaschke, *Journal of Colloid and Interface Science*, 1969, **29**, 710-719.